Continental Shelf Research 34 (2012) 53–63

Contents lists available at SciVerse ScienceDirect

Continental Shelf Research

journal homepage: www.elsevier.com/locate/csr

Research papers

Tide-induced suspended sediment transport: Depth-averaged concentrations and horizontal residual fluxes

Qian Yu [a,b,*], Ya Ping Wang [a], Burg Flemming [b], Shu Gao [a]

[a] MOE Laboratory for Coast and Island Development, Nanjing University, 210093 Nanjing, China
[b] Senckenberg Institute, D-26382 Wilhelmshaven, Germany

ARTICLE INFO

Article history:
Received 6 June 2011
Received in revised form
29 November 2011
Accepted 30 November 2011
Available online 8 December 2011

Keywords:
Suspended sediment concentration/flux
Resuspension
Advection
Tidal pumping
Jiangsu Coast

ABSTRACT

In coastal and estuarine waters, depth-averaged suspended sediment concentration (DASSC) at a fixed observation site has two sources: local resuspension and advection along a horizontal gradient. The empirical decomposition method can separate the horizontal residual suspended sediment flux (HRF) into several terms, e.g., Eulerian flux, Stokes' drift and tidal pumping. A simple depth-averaged 1D model is solved analytically for an observational site over one semi-diurnal tidal cycle to explore the determinants of the forcing factors comprising residual, M2 and M4 current velocities, mean water depth, M2 tidal amplitude and the DASSC gradient. The analytical solutions provide clear physical explanations of tidal DASSC variations and HRF. The solutions are applied to fit and explain the observations at a fixed station in a macro-tidal channel located along the Jiangsu Coast, China. The results suggest a dependence of the M4 DASSC variation on resuspension induced by the M2 velocity, and the dependence of the M2 DASSC variation on the advection and resuspension induced by the interaction between the M2 and M4 velocities. The horizontal DASSC gradient results in large seaward tidal pumping, which is offset by the landward Lagrangian flux to produce a reduced landward HRF.

1. Introduction

Understanding the tide-induced behavior of suspended sediment dynamics is vital for morphological, environmental and ecological reasons (Dyer, 1997; Prandle, 1997). There are two key issues in this respect, namely, suspended sediment concentration (SSC), and horizontal residual suspended sediment flux (HRF). The former plays an important role in absorbing and scattering light, and hence influences biological production (Tian et al., 2009), whereas the latter is essential in determining the fate of the sediment and its associated contaminants, including carbon in the context of the global consequences of anthropogenic change (Jay et al., 1997). For these reasons, SSC and current velocity time series are commonly measured at some fixed field stations during coastal and estuarine hydrodynamic surveys. From such data, the HRF can then be calculated for those locations by the integration of the observed SSC and velocity over individual tidal cycles. Consequently, the interpretation and prediction of SSC and HRF are based on both empirical and theoretical considerations.

By means of harmonic analysis of the tidal current signal, the observed SSC can be decomposed into several periodic components. In areas dominated by the M2 tide and its overtide, field data analysis showed that most of the SSC variance occurs at the M2 and M4 frequencies (Sternberg et al., 1985; van de Kreeke et al., 1997; Guezennec et al., 1999; van de Kreeke and Hibma, 2005). Theoretically, there are two potential sources for the suspended sediment at the observational point: localized sediment resuspension and horizontal advection. On this basis, Weeks et al. (1993) established a conceptual model to distinguish between these contributions. They suggested that, in an environment dominated by the M2 tidal current and characterized by a horizontal SSC gradient, the M2 SSC variation is due to advection along this gradient, whereas the M4 SSC variation is caused by localized resuspension as it is dependent on the magnitude but not the direction of the M2 current. This concept has been used to separate the contributions of advection and resuspension from observed SSC time series (Jago and Jones, 1998; Ellis et al., 2004; Jago et al., 2006; Krivtsov et al., 2008). Furthermore, a similar consideration has been suggested in relating the M2 SSC signal to advection and the M4 SSC signal to resuspension (Sternberg et al., 1985; Sanford and Halka, 1993; van de Kreeke et al., 1997; van de Kreeke and Hibma, 2005). However, in some cases, more factors act on the system, which can then not be neglected, e.g., residual and M4 tidal currents. The question thus arises as how to specify the interaction of the different forcing factors in order to assess their individual contributions to the tidal SSC variation.

In principle, there is no problem in calculating suspended sediment fluxes from field measurements of SSC and current

* Corresponding author at: MOE Laboratory for Coast and Island Development, Nanjing University, 210093 Nanjing, China. Tel.: +86 25 83597308; fax: +86 25 83595387.
E-mail address: qianyu.nju@gmail.com (Q. Yu).

0278-4343/$ - see front matter © 2011 Elsevier Ltd. All rights reserved.
doi:10.1016/j.csr.2011.11.015

velocity. In analogy to the estuarine salt transport decomposition method (Dyer, 1974; Fischer, 1976), the suspended sediment flux averaged over a tidal cycle, here called HRF, can be quantified as follows (Dyer, 1997):

$$F=\frac{1}{T}\int_0^T\int_0^H UC\,dz\,dt=\underbrace{C_0U_0H_0}_{F1}+\underbrace{C_0\overline{U_tH_t}}_{F2}+\underbrace{U_0\overline{H_tC_t}}_{F3}+\underbrace{H_0\overline{U_tC_t}}_{F4}+\underbrace{\overline{C_tU_tH_t}}_{F5}+\underbrace{H_0\langle\overline{U}_d\overline{C}_d\rangle}_{F6}+\underbrace{H_0\langle\overline{U_{dt}C_{dt}}\rangle}_{F7} \quad (1)$$

where C is the SSC, U is the current velocity, T is the tidal period, H is the water depth, the subscript 0 denotes the mean value over time and space, the subscript t denotes the vertically averaged tidal variation, the subscript d denotes the deviations from the vertical means and the subscript dt denotes the temporal deviations from the tidal averaged deviations from the vertical means. Angled brackets ($\langle\ \rangle$) and overbars ($\overline{\ }$) signify the means over the depth and the tidal cycle, respectively.

Each decomposed term represents a particular contribution related to a certain physical process (Dyer, 1997). The first term (F1) represents the non-tidal drift, called the Eulerian flux, while the second term (F2) is the flux induced by the Stokes' drift. The two terms denote the residual flow of water and the tidally and vertically averaged SSC to provide the advective sediment flux (the Lagrangian flux). The terms F3–F5 are the tidal pumping terms that are produced by the phase differences between the depth-averaged suspended sediment concentration (DASSC), the depth-averaged velocity and the tidal elevation. Term F6 indicates the tidally averaged vertical circulation, while term F7 arises from the changing forms in the vertical distribution of SSC and velocity.

This decomposition method has been applied widely to the study of sediment flux patterns (Uncles et al., 1985a,b; Su and Wang, 1986; Uncles and Stephens, 1993; Barua et al., 1994; Pino Q et al., 1994; Li and Chen, 1998; Wu et al., 2001; Ganju et al., 2005). By comparing the values of the decomposed terms, the relative importance of different processes can be assessed. One important application of the decomposition method, for example, is to help understand the formation mechanism of estuarine turbidity maxima (ETM) (Dyer, 1997). Especially in well-mixed water bodies, tidal pumping plays a primary role for the maintenance of the ETM, this feature having been revealed by various observational and numerical modeling approaches (Allen et al., 1980; Uncles and Stephens, 1989; Brenon and Le Hir, 1999; Le Hir et al., 2001).

However, although each decomposed term can be related to particular physical processes, the quantitative contributions of the various forcing factors are not at clear. For example, the tidal pumping terms are generally explained by the phase differences between the DASSC, the depth-averaged velocity and the tidal elevation. But the DASSC is also a production of external forcing factors, including residual and tidal currents, tidal heights and horizontal advection. Thus, in order to obtain a comprehensive understanding, the tidal pumping terms must consider the original forcing factors acting at a particular site. This, however, also requires a clarification of how to define the physical basis of each factor for the decomposition procedure.

To solve these issues, several numerical and analytical modeling approaches have been suggested. Thus, Bass et al. (2002) established a numerical model to study the response of SSC to tidal currents by assuming a constant horizontal SSC gradient, the results being then fitted to the observations, thereby supporting the SSC separation concept of Weeks et al. (1993). Although numerical modeling has the advantage of interpreting field observations and analyzing the sensitivity to different parameters, analytical models are better able to provide insights into the generic physics of system evolution (Dronkers, 2005). The analytical solutions of DASSC driven by several tidal constituents (e.g., M2, M4) have been investigated by Groen (1967) and Prandle (1997) without, however, considering the contribution of advection. Stanev et al. (2007) and Cheng and Wilson (2008) took horizontal advection into account and solved the depth-averaged one-dimensional (1D) suspended sediment transport equation for a particular site, but neglected the residual current velocity and water depth variation. While Cheng and Wilson (2008) compared their solution with numerical modeling results, none of the above analytical solutions were directly compared with field observations.

The analytical formula of HRF is based on the solution of DASSC. Because of the lag response of SSC to the tidal current (Yu et al., 2011), the horizontal transport of suspended sediment is more complicated than that for bedload (van de Kreeke and Robaczewska, 1993; van Maren et al., 2004). As advection is not included in the DASSC solutions of Groen (1967) and Hoitink et al. (2003), their HRF solutions can not be applied to spatially heterogeneous areas. This effect, on the other hand, was considered by Cheng and Wilson (2008), but because they neglected the contributions of residual current velocity and water depth variation, some decomposition terms of the HRF in Eq. (1), which represent the Stokes' drift and a part of the tidal pumping, can not be specified. Pritchard (2005) provided semi-analytical solutions for HRF, but these are relatively complex and hence difficult to directly implement in practice.

As a result, improved analytical solutions of DASSC and HRF are required to take account of both the contributions of advection and resuspension, and, more importantly, the solutions need direct field evidence not only for validation but also for providing new insights into the local sediment transport patterns. The present study attempts to solve the 1D depth-averaged suspended sediment transport equation for a site with a more comprehensive inclusion of forcing factors (e.g., M2 tidal elevation, residual, M2 and M4 tidal currents and a horizontal DASSC gradient). On this basis, the HRF is then formulated analytically and the physical meanings of its first 5 decomposition terms are clarified. The solutions are verified by field observations at an anchor station in a macro-tidal embayment located along the Jiangsu Coast, China.

2. Analytical solution

In this part, a procedure for the analytical solution to investigate the tidal response of DASSC and HRF is presented. Three basic processes are involved, including advection of a horizontal DASSC gradient, local resuspension and deposition. For the sake of simplification, the solution is based on a depth-averaged 1D model, and has been designed to provide single-point analytical expressions of DASSC and HRF over one semi-diurnal tidal cycle. This is achieved by means of simplified parameterizations of the above three basic processes. The single-point analytical solutions can thus be used for a direct comparison with observations at fixed field stations, the tidal current motion being characterized as a 1D system.

At first, a lateral homogeneous environment is assumed where the longitudinal 1D depth-averaged suspended sediment transport model is defined as

$$\frac{\partial\langle C\rangle H}{\partial t}=-\frac{\partial\langle UC\rangle H}{\partial x}+\text{Resuspension}+\text{Deposition} \quad (2)$$

with C as the SSC and U as the current velocity, both being functions of time (t) and horizontal distance (x) and H as the water depth. The horizontal diffusion term is neglected (Bass et al., 2002; Stanev et al., 2007). The first term on the right-hand

side (RHS) represents the contribution from horizontal advection. In addition, simultaneous local resuspension and deposition are assumed (Sanford and Halka, 1993) and width variations in velocity and SSC have been suppressed for simplicity.

The horizontal advection term in Eq. (2) can be decomposed as follows:

$$\frac{\partial \langle UC\rangle H}{\partial x} = \frac{\partial \langle U\rangle \langle C\rangle H}{\partial x} + \frac{\partial \langle U_d C_d\rangle H}{\partial x} \tag{3}$$

The second term in the RHS of Eq. (3) indicates the nonlinear interaction between the vertical velocity and SSC profiles. For the sake of simplicity, the third term in Eq. (3) is not considered further as in other depth-averaged models (Dronkers, 1986; Uncles and Stephens, 1989; Cheng and Wilson, 2008). Eq. (3) then reduces to

$$\frac{\partial \langle UC\rangle H}{\partial x} = \frac{\partial \langle U\rangle \langle C\rangle H}{\partial x} = \langle U\rangle H\frac{\partial \langle C\rangle}{\partial x} + \langle C\rangle \frac{\partial \langle U\rangle H}{\partial x} \tag{4}$$

The resuspension rate due to the tidal current is written as (Cheng and Wilson, 2008):

$$\text{Resuspension} = B\langle U\rangle^2, \quad B = \frac{M\rho C_D}{\tau_{cr}} \tag{5}$$

where M is an erosion constant, and C_D is the drag coefficient applicable to the depth-averaged velocity, and τ_{cr} is the critical erosion shear stress. For the sake of simplicity, M, C_D and τ_{cr} are assumed to be constant over time and space. Coefficient B thus becomes a constant that represents the resuspension capacity.

The deposition rate is given by

$$\text{Deposition} = W_s C_{bed} = D\langle C\rangle H, \quad D = W_s\frac{C_{bed}}{\langle C\rangle H} \tag{6}$$

where W_s is the sediment setting velocity, and C_{bed} is the near-bed SSC. For the sake of simplicity, it is assumed that the settling velocity and the ratio between the near-bed SSC (C_{bed}) and the vertical sediment inventory ($\langle C\rangle H$) are constant over time and space. Coefficient D thus also becomes a constant, which represents the deposition capacity.

Combining Eqs. (2)–(6) with the continuity equation for flowing water

$$\frac{\partial \langle U\rangle H}{\partial x} = -\frac{\partial H}{\partial t} \tag{7}$$

a simple form of the continuity equation for suspended sediment is obtained

$$\frac{\partial \langle C\rangle}{\partial t} + D\langle C\rangle = -\langle U\rangle\frac{\partial \langle C\rangle}{\partial x} + \frac{B}{H}\langle U\rangle^2 \tag{8}$$

In this equation, three basic processes, namely advection of a horizontal DASSC gradient, local resuspension and deposition are described. The second term on the left-hand side (LHS) represents the contribution of deposition, which is proportional to the DASSC, and the first and second terms of the RHS stand for the contributions of advection and resuspension, respectively. The effects of advection on the DASSC depend on the velocity and the horizontal DASSC gradient, the latter being hard to estimate analytically in practice. A substitute method to simulate this gradient is to find an approximate formula using empirical parameters from the study site. For example, the gradient can be assumed to be uniform and hence represented by a constant value (Weeks et al., 1993; Bass et al., 2002), or to be expressed as a combination of several temporal harmonic terms (Cheng and Wilson, 2008). At the study site, the tidal characteristics of current velocity and water depth can be obtained through harmonic analysis of observational data. By parameterizing the horizontal DASSC gradient, $\langle U\rangle$, and H in the harmonic series, the RHS of the Eq. (8) can be written as a summation of a trigonometric Fourier series only associated with time

$$\frac{\partial \langle C\rangle}{\partial t} + D\langle C\rangle = \sum_{i=1} A_i \cos(\omega_i t + \psi_i) \tag{9}$$

where A_i, ω_i and ψ_i are the amplitude, frequency and phase of the ith forcing harmonics, respectively. The general analytical solution of Eq. (9) can now be written as:

$$\langle C\rangle = Se^{-Dt} + \sum_{i=1}\frac{A_i}{\sqrt{\omega_i^2+D^2}}\cos(\omega_i t + \psi_i - \theta_i), \quad \theta_i = \tan^{-1}\frac{\omega_i}{D} \tag{10}$$

where S is an integral constant, and when the evolution of $\langle C\rangle$ tends to be stable, the first term of the RHS of Eq. (10) becomes trivial and can be neglected. This solution depicts the temporal evolution of the DASSC at the study site.

Comparing the above two equations indicates that the ith harmonic of $\langle C\rangle$ in the second term of the RHS of Eq. (10) responds to the ith forcing harmonic in the RHS of Eq. (9) with the same frequency ω_i but with the amplitude reduced by the factor $(\omega_i^2+D^2)^{1/2}$, on account of which the phase lags by θ_i.

In this study, the particular case is investigated where the transformation from the RHS of Eq. (8) to the harmonic series in the RHS of Eq. (9) can be specified. At first, because the dominant astronomical tide along much of the world's coasts is the semi-diurnal lunar tide (M2), the rectilinear tidal velocity can be modeled by a superposition of the M2 tide and its most significant overtide M4 (Friedrichs and Aubrey, 1988)

$$\begin{aligned}\langle U\rangle &= u_0 + u_1\cos(\omega t+\varphi_1) + u_2\cos(2\omega t+\varphi_2) \quad \hat{u}_0 = u_0/u_1\\ &= u_1[\hat{u}_0 + \cos(\omega t+\varphi_1) + \hat{u}_2\cos(2\omega t+\varphi_2)] \quad \hat{u}_2 = u_2/u_1\end{aligned} \tag{11}$$

where u_0, u_1 and u_2 are the depth-averaged amplitudes of the residual, M2 and M4 velocities, respectively, φ is the phase of tidal velocity, and ω is the M2 tidal frequency. Since the amplitudes of residual and M4 velocities are typically one order of magnitude lower than the M2 amplitude, u_0 and u_2 are normalized by u_1 as $\hat{u}_0$ and $\hat{u}_2$, respectively. These dimensionless variables are typically in the order of 0.1.

Similarly, the water depth can be modeled by a superposition of the M2 and M4 tides

$$\begin{aligned}H &= h_0 + h\cos(\omega t+\phi) + h_2\cos(2\omega t+\phi_2) \quad \hat{h} = h/h_0\\ &= h_0[1+\hat{h}\cos(\omega t+\phi)]\end{aligned} \tag{12}$$

where h_0 is the average water depth, and h and h_2 are the amplitudes of the M2 and M4 tidal elevations, respectively, and ϕ is the phase of the tidal elevation. In coastal and estuarine environments, it is assumed that h_0 is significantly larger than h, and h is significantly larger than h_2. Therefore, the contribution of the M4 tidal elevation can be neglected, and the dimensionless $\hat{h}$ is typically one order lower than 1. The inverse of the water depth can be approximated by

$$\frac{1}{H} = \frac{1}{h_0[1+\hat{h}\cos(\omega t+\phi)]} = \frac{1}{h_0}[1-\hat{h}\cos(\omega t+\phi)] \tag{13}$$

Because the spatial information on the DASSC is frequently unavailable in the field, a constant gradient (k) over time at the study site is assumed for the sake of simplicity in accordance with previous models (Prandle, 1997; Bass et al., 2002; Hill et al., 2003). The particular value of k can be attributed to the spatial heterogeneity of tidal currents, wave activity, sediment supply or water depth, and is especially valid for fine-grained materials (Prandle, 1997)

$$\frac{\partial \langle C\rangle}{\partial x} = k \tag{14}$$

Substituting Eqs. (11), (13) and (14) to Eq. (8), and neglecting the higher order (>1) trivial terms, the solution for the temporal

evolution of DASSC is specified as:

$$\langle C\rangle = \sum_{i=1}^{8} \mathrm{E}i = \sum_{i=1}^{8} \frac{A_i}{\sqrt{\omega_i^2+D^2}} \cos(\omega_i t+\psi_i-\theta_i), \quad \theta_i = \tan^{-1}\frac{\omega_i}{D} \tag{15}$$

The solution consists of eight harmonic terms (E1–E8), their amplitude, frequency and phase being listed in Table 1. Each harmonic represents one or more process affecting the DASSC variation (see Appendix A). In terms of this solution, the contributions of the forcing factors, which comprise the residual, M2 and M4 current amplitudes and phases, the mean water depth, the M2 tidal amplitude and phase, and the DASSC gradient, can be determined.

In accordance with the second column in Table 1, it can be shown that k/u_1 and B/h_0 are comparable parameters, representing the relative importance of the horizontal advection due to the SSC gradient and the local resuspension, respectively.

The analytical formula of HRF is, in turn, achieved by integrating the known analytical formulas of DASSC (Eq. (15)) and current velocity (Eq. (11)) over the vertical domain and the M2 tidal period. Because of the vertically averaged model, the first five terms (F1–F5) of the HRF decomposition can be determined analytically for physical interpretations. Terms F6 and F7, which are related to the vertical deviations, are not covered by the present study. Neglecting the higher order (>2) trivial terms, the decomposition terms (F1–F5) are written as:

$$\mathrm{F1} = \frac{u_1^3 h_0}{D}\left(\frac{1}{2}\frac{B}{h_0}\hat{u}_0 - \frac{k}{u_1}\hat{u}_0^2\right) \tag{16}$$

$$\mathrm{F2} = \frac{u_1^3 h_0}{2D}\cos(\varphi_1-\phi)\left(\frac{1}{2}\frac{B}{h_0}\hat{h} - \frac{k}{u_1}\hat{u}_0\hat{h}\right) \tag{17}$$

$$\mathrm{F3} = -\frac{u_1^3 h_0}{2\sqrt{\omega^2+D^2}}\frac{k}{u_1}\hat{u}_0\hat{h}\cos(\varphi_1-\phi-\theta_\omega) \tag{18}$$

Table 1
The coefficients of the trigonometric Fourier series in Eq. (15). (See text for description.)

	A_i/u_1^2	ω_i	ψ_i
E1	$-\frac{k}{u_1}\hat{u}_0+\frac{1}{2}\frac{B}{h_0}$	0	0
E2	$-\frac{k}{u_1}+2\frac{B}{h_0}\hat{u}_0-\frac{1}{2}\frac{B}{h_0}\hat{h}\cos(\phi-\varphi_1)$	ω	φ_1
E3	$\frac{B}{h_0}\hat{u}_2$	ω	$\varphi_2-\varphi_1$
E4	$-\frac{1}{4}\frac{B}{h_0}\hat{h}$	ω	ϕ
E5	$-\frac{k}{u_1}\hat{u}_2$	2ω	φ_2
E6	$\frac{1}{2}\frac{B}{h_0}$	2ω	$2\varphi_1$
E7	$\frac{B}{h_0}\hat{u}_2$	3ω	$\varphi_1+\varphi_2$
E8	$-\frac{1}{4}\frac{B}{h_0}\hat{h}$	3ω	$2\varphi_1+\phi$

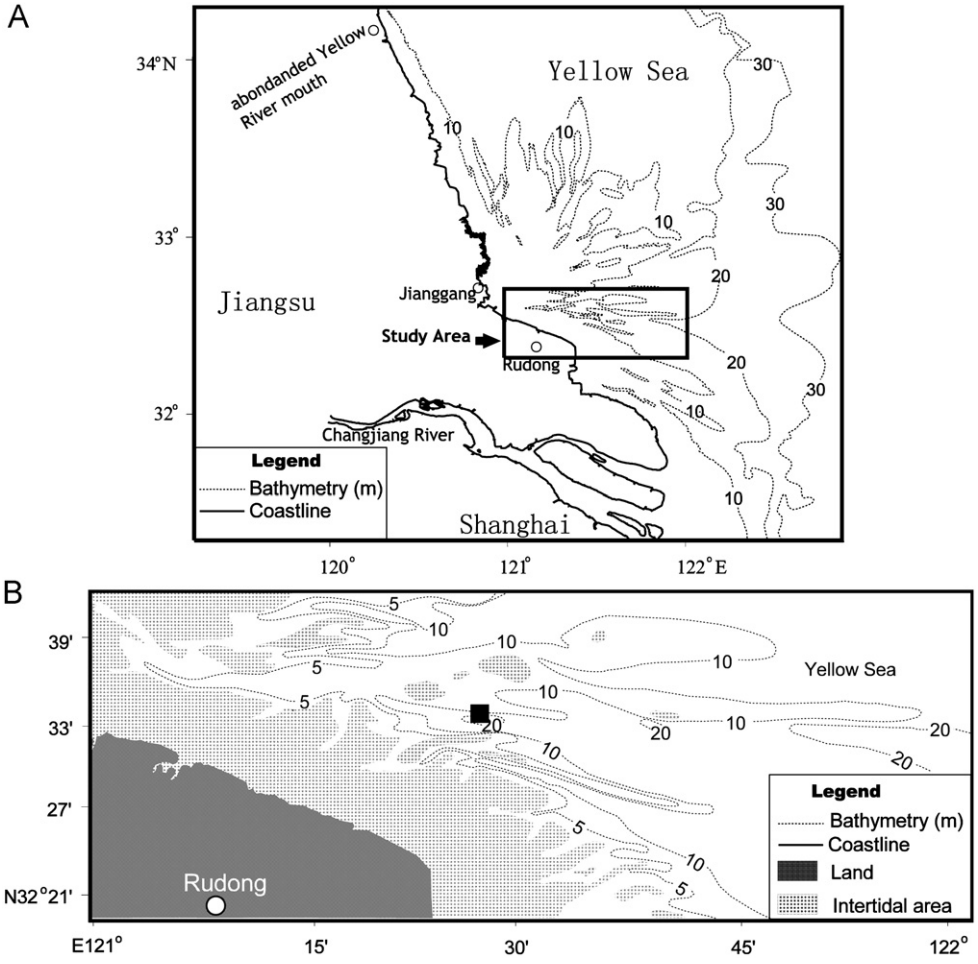

Fig. 1. Bathymetric map of the study area. The filled square is the observation site.

$$\mathrm{F4}=\frac{u_1^3h_0}{2\sqrt{\omega^2+D^2}}\left[\left(-\frac{k}{u_1}+2\frac{B}{h_0}\hat{u}_0-\frac{1}{2}\frac{B}{h_0}\hat{h}\cos(\phi-\varphi_1)\right)\cos\theta_\omega+\frac{B}{h_0}\hat{u}_2\cos(2\varphi_1-\varphi_2+\theta_\omega)-\frac{1}{4}\frac{B}{h_0}\hat{h}\cos(\phi-\varphi_1-\theta_\omega)\right]+\frac{u_1^3h_0}{2\sqrt{4\omega^2+D^2}}\left[-\frac{k}{u_1}\hat{u}_2^2\cos\theta_{2\omega}+\frac{1}{2}\frac{B}{h_0}\hat{u}_2\cos(2\varphi_1-\varphi_2-\theta_{2\omega})\right] \tag{19}$$

$$\mathrm{F5}=\frac{u_1^3h_0}{8\sqrt{4\omega^2+D^2}}\frac{B}{h_0}\hat{h}\cos(\varphi_1-\phi-\theta_{2\omega})-\frac{u_1^3h_0}{4\sqrt{\omega^2+D^2}}\frac{k}{u_1}\hat{u}_2\hat{h}\cos(\varphi_1-\varphi_2+\phi-\theta_\omega) \tag{20}$$

where $\theta_\omega=\tan^{-1}(\omega/D)$, $\theta_{2\omega}=\tan^{-1}(2\omega/D)$, representing the phase lag of SSC to the forcing factors in the M2 and M4 frequencies, respectively. The interpretations of F1–F5 can be found in Appendix B.

In practice, when current velocity, water depth and SSC are measured at a fixed site, the analytical solutions can be applied in the following procedure. In a first step, the values of u_0, u_1, u_2, h_0, h, φ_1, φ_2 and ϕ are identified by harmonic analysis of the measured tidal current and the water depth at the study site. Three free parameters, however, can not be identified independently and thus need to be calibrated by fitting the prediction to the observed DASSC variations: the DASSC gradient k, the resuspension coefficient B and the deposition coefficient D. Then, the temporal variation of DASSC is specified and its eight decomposed terms in Eq. (15) are related to the special effects of the different forcing factors with clear physical meanings. The best fit parameters are applied to Eqs. (16)–(20), and then, HRF is predicted and interpreted theoretically.

3. Observations and applications

Hydrodynamic observations were carried out in a tidal channel located along the Jiangsu Coast, China (Fig. 1). Little fresh water flows into the study area, suggesting a well-mixed water body. The study area is characterized by a large tidal range and strong tidal currents of up to 7 m and 2 m s^{-1}, respectively. The M2 tide is the dominant tidal constituent. The bed mainly consists of silt and very fine sand, which are both mostly transported as suspended loads. Samples collected at the site have a mean grain size of 3.8φ. Field observations and remote sensing results based on TM images shown the on-shore increase of SSC along Jiangsu Coastal Sea (Xin et al., 2010).

A ship-mounted downward-looking acoustic Doppler current profiler (ADCP) (600 kHz, RDI) was deployed over a spring tidal period between 15 and 16 July 2003 at an anchor station (121°27′E, 32°34′N) with a mean water depth of about 20 m (Fig. 1). Local wind waves are <0.5 m in height and are therefore of minor importance for sediment transport in the channel. Current velocity and acoustic backscatter intensity profiles were recorded every 30 s. During the observation, 55 water samples from different water layers were collected at different times. These were subsequently filtered through pre-weighed filters of 0.45 μm aperture. The filters plus sediment were dried and weighed to determine the SSC, which was then used to calibrate the acoustic signal strength of the ADCP. A linear regression equation was established between SSC (C, in mg l^{-1}) and the ADCP backscatter intensity (EI in dB) (Fig. 2)

$$\log_{10}(C)=-4.8557+0.0788\mathrm{EI}\quad R=0.86 \tag{21}$$

During the observational period, the tidal velocities were almost rectilinear directed east–west along the channel axis. Fig. 3 shows the temporal evolution of the vertical current speed and SSC profiles, the latter being estimated from the backscatter intensity following Eq. (21). To remove some of the ruggedness in the high-frequency records, the water depth and the vertically averaged SSC were smoothed using a 10 min window (Fig. 4, middle and lower panels). The current speeds and directions were also averaged every 10 min. According to the method of You (2005), the main tidal current direction was determined as being 93° clockwise from the north, the measured velocity being then projected in this direction (Fig. 4, upper panel). The projected velocity has positive values towards the sea and the fit by Eq. (11) represents the combined residual, M2 and M4 velocities

$$\begin{aligned}\langle U\rangle&=-0.08+1.32\cos(\omega t+115^\circ)+0.11\cos(2\omega t+219^\circ)\\&=1.32[-0.061+\cos(\omega t+115^\circ)+0.083\cos(2\omega t+219^\circ)]\end{aligned} \tag{22}$$

The observed and fitted velocities have a high degree of consistency (Fig. 4, upper panel). The fitted result (Eq. (22)) suggests (1) that the dominant M2 velocity amplitude is one order of magnitude larger than the residual and M4 velocities;

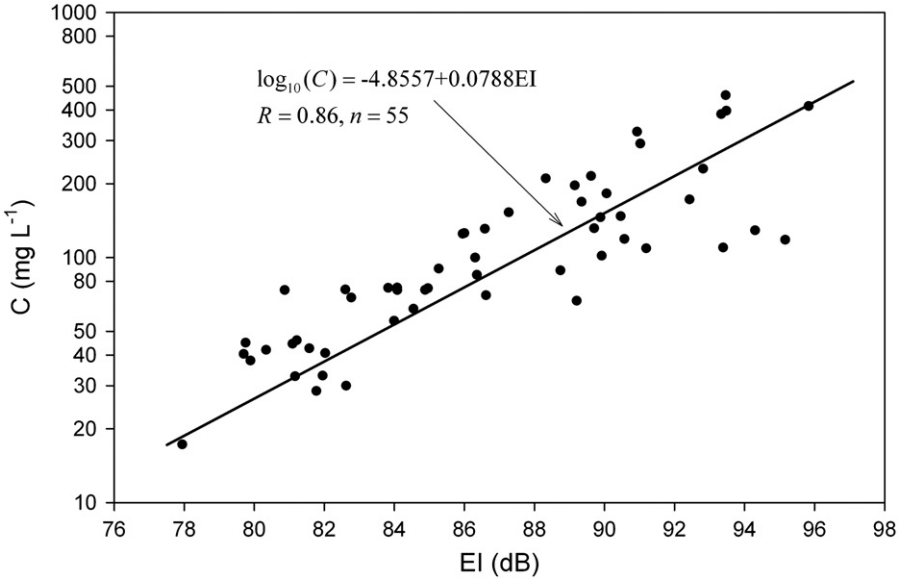

Fig. 2. The relationship between SSC (C in mg l^{-1}) and ADCP backscatter signal intensity (EI in dB).

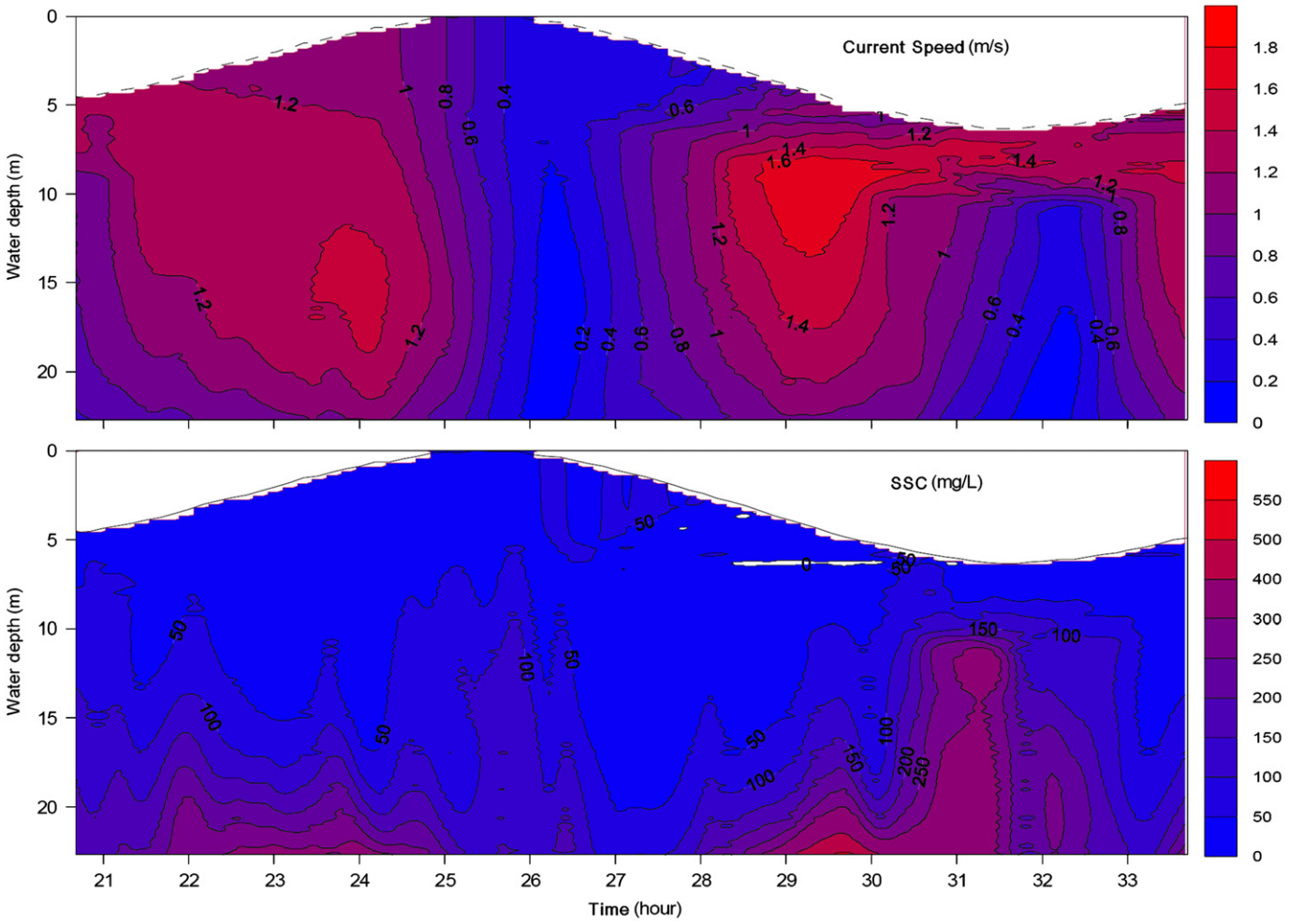

Fig. 3. Observed current speed and SSC during a tidal cycle.

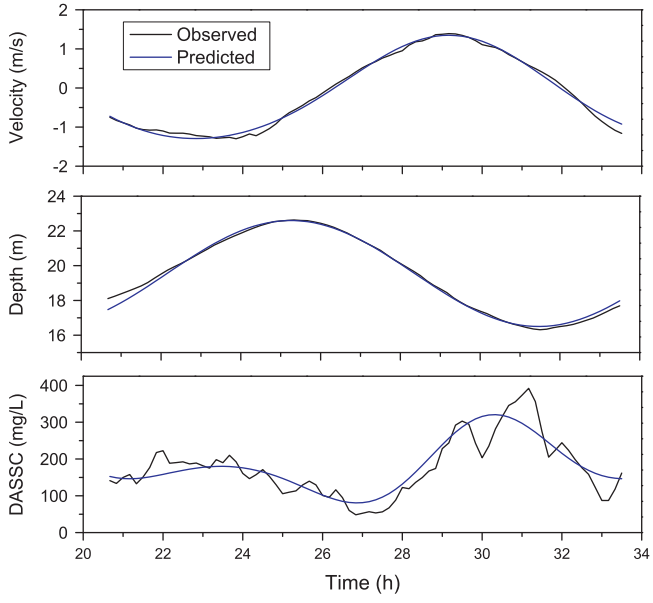

Fig. 4. Observed and predicted current velocity, water depth and DASSC. Positive velocities are directed seaward.

(2) that the phase difference between the M2 and M4 velocities is ebb dominated; and (3) that the residual velocity is directed landward and has the close amplitude as the M4 velocity.

Similarly, the observed water depth is fitted by the combined mean depth and M2 tidal elevation following Eq. (12) (Fig. 4, middle panel)

$$H = 19.55 + 3.05\cos(\omega t + 225^\circ) = 19.55[1 + 0.156\cos(\omega t + 225^\circ)] \quad (23)$$

The M2 tidal range is 6.1 m, its phase leading the M2 velocity by 112°, a condition midway between standing and progressive tidal wave and landward Stokes' drift of the water.

Because no spatial DASSC information was available, and the estimation of the mean sediment settling velocity and erosion constant are difficult, the three parameters (k, B and D) needed to be calibrated. The predicted DASSC based on the analytical solution in Eq. (15) was fitted to the ADCP concentration data for optimization. A similar procedure as that used to determine the free parameters by fitting the modeling results to the observational data has previously been applied in other numerical modeling approaches (Sanford and Halka, 1993; Jago and Jones, 1998; Bass et al., 2002; Yang and Hamrick, 2003). Because the best fit parameters encapsulate a number of assumptions and simplifications made in the analytical solution, these parameters may not represent actual values, but are nevertheless useful in interpreting the measured concentration signal.

Before fitting, the ranges of the three parameters must be constrained. The observed tidally averaged DASSC was about 200 mg l^{-1} and the tidal excursion distance about 20 km. As a result, the maximum possible value of the gradient is about

1.0×10^{-5} kg m^{-4}, and the limits for k were thus set at -2.0×10^{-5} and 2.0×10^{-5} kg m^{-4}. Amos et al. (1992) found that the erosion constant M in Eq. (5) ranges between 2.0×10^{-5} and 3.5×10^{-3} kg m^{-2} s^{-1}. In the present study, this range was reduced to 10^{-5} and 5.0×10^{-3} kg m^{-2} s^{-1}, and a τ_{cr} of 0.25 N m^{-2} for sand–mud mixtures (van Ledden et al., 2004) and a C_D of 2.5×10^{-3} assumed (Soulsby, 1997). Thus, based on Eq. (5), the resuspension coefficient B was constrained between 10^{-4} and 5.0×10^{-2} kg s m^{-4}. The lower limit for the sediment settling velocity was set at 0.07 mm s^{-1} (corresponding to a grain size of about 10 μm, cf. Gibbs et al., 1971), the upper limit at 3 mm s^{-1} (corresponding to that of large flocs; Hill and McCave, 2001). The ratio between near-bed SSC and DASSC, which was estimated from the observed SSC profiles, has a mean value of 4.59. In terms of Eq. (6) and using the mean depth of 19.55 m, the deposition coefficient D ranges between 1.6×10^{-5} and 7.0×10^{-4} s^{-1}.

The best fit prediction of DASSC by the analytical solution is plotted in the lower panel of Fig. 4. Compared with the observations, the prediction shows reasonable agreement in that, besides the high-frequency fluctuations in the measured data, the main DASSC variance is represented by the prediction. The calibrated parameters of k, B and D have reasonable values (Table 2). The best fit k of -8.8×10^{-6} kg m^{-4} indicates the landward increase in DASSC by 88 mg l^{-1} every 10 km. This landward increase in DASSC in coastal tidal channels had already been recognized by Postma (1961) in the Dutch Wadden Sea, and is also consistent with the general patterns of the spatial distribution of the Jiangsu Coastal Sea (Xin et al., 2010). The best fit B of 4.2×10^{-4} kg s m^{-4} and D of 1.0×10^{-4} s^{-1} are related to an erosion constant of about 4.2×10^{-5} kg m^{-2} s^{-1} and a sediment settling velocity of about 0.42 mm s^{-1}, respectively. The two parameters k/u_1 and B/h_0 are 6.7×10^{-6} and 2.2×10^{-5} kg s m^{-5}, respectively, indicating comparable contributions of horizontal advection due to the SSC gradient and local resuspension.

Based on Eq. (15), the DASSC can be decomposed into eight terms (E1–E8). The tidally averaged DASSC (E1) of observations and predictions are 177.6 and 181.7 mg l^{-1}, respectively. Applying the best fit parameters to Eq. (A1) in Appendix A illustrates that advection (the first term of the RHS in the equation) contributes -7.1 mg l^{-1} because the residual current comes from a low concentration area, and that local resuspension contributes 188.8 mg l^{-1}.

The tidally varying terms of E2–E8 are shown in Fig. 5. E6, E2 and E3 have amplitudes of 63.3, 44.2 and 18.2 mg l^{-1}, respectively, making the largest contribution to the total variation. The relative importance of Ei (i=2–8) in Eq. (15) can be evaluated as the ratio between the amplitude of Ei and the sum of the amplitudes of E2–E8. The results suggest that the ratios for E6, E2 and E3 are 42.7%, 29.8% and 12.3%, respectively, the sum of the three ratios amounting to 84.8%. E6 has the M4 frequency, and E2 and E3 have the M2 frequency.

On the basis of the analytical solution (Table 1 and Appendix A), it is known that E6 represents the M4 variation of the DASSC induced by the M2 current resuspension, which corresponds to the local component in the concept of Weeks et al. (1993). Because of the trivial parameters $\hat{u}_0$ and $\hat{h}$ and the comparable values of k/u_1 and B/h_0, the amplitude of E2 are dominated by k/u_1 (Table 1), this in-phase variation with the M2 velocity being thus mainly attributable to the advection effect. Ebb currents bring high concentration waters to the observation site, resulting in a higher DASSC during the ebb than during the flood tide. If the residual velocity and the water depth variance are excluded, E2 is consistent with the advection component of Weeks et al. (1993). E3, which is due to the resuspension induced by the interaction of the M2 and M4 velocities, also has an M2 frequency, its relative importance being controlled by $\hat{u}_2$. Therefore, the M2 variations of DASSC are not only controlled by advection effects, but are also related to the contributions of the residual velocity, the water depth variance, and, especially, the local resuspension.

In Table 2, HRF and its decomposition terms (F1–F5) are calculated on the basis of the observations, the Prediction1 using the best fit parameters to Eqs. (16)–(20) producing reasonable results. It should be noted that here F6 and F7 are neglected and HRF is the sum of F1–F5. The Eulerian flux (F1), which is driven by the landward residual velocity and the tidally averaged DASSC, is directed landward. Because of the phase difference of 112° between the M2 velocity and the M2 elevation, the Stokes' drift (F2) is also landward directed. F3 is small, and F4 dominates the tidal pumping. Appling the best fit parameters in Eq. (19), it is found that the landward positive DASSC gradient is the most

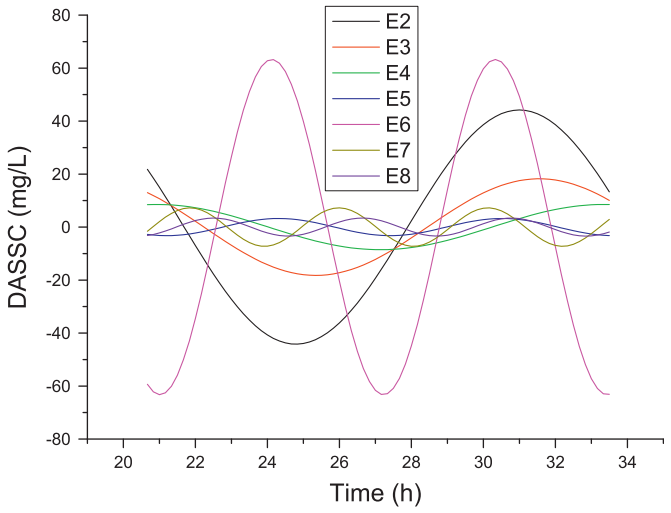

Fig. 5. Periodic decomposition terms (E2–E8) in Eq. (15) using the best fit parameters. E2–E8 are the harmonic terms of DASSC variations shown in Table 1.

Table 2
The tide- and depth-averaged SSC (E1), HRF and its decomposition terms (F1–F5) at the observation site. Observation data are listed on the first row. Prediction1 uses the three best fit parameters (DASSC gradient k, resuspension coefficient B and deposition coefficient D), Prediction2 forces the zero k, representing the non-advection condition, Prediction3 forces the zero k and the half D, representing the finer sediment condition, and Prediction4 forces the zero k and the double D, representing the coarser sediment condition. Positive values of sediment flux denote seaward.

	$k\times10^6$ (kg m^{-4})	$B\times10^4$ (kg s m^{-4})	$D\times10^4$ (s^{-1})	E1 (mg l^{-1})	F1 (kg m^{-1} s^{-1})	F2 (kg m^{-1} s^{-1})	F3 (kg m^{-1} s^{-1})	F4 (kg m^{-1} s^{-1})	F5 (kg m^{-1} s^{-1})	HRF (kg m^{-1} s^{-1})
Observation				177.6	−0.277	−0.133	0.009	0.358	−0.074	−0.117
Prediction1	−8.8	4.2	1.0	181.7	−0.284	−0.137	0.008	0.432	−0.062	−0.043
Prediction2	0	4.2	1.0	188.8	−0.295	−0.142	0.000	−0.077	−0.064	−0.578
Prediction3	0	4.2	0.5	363.4	−0.590	−0.284	0.000	−0.131	−0.066	−1.071
Prediction4	0	4.2	2.0	90.9	−0.148	−0.071	0.000	−0.064	−0.054	−0.337

important reason for the positive sign of F4 (seaward). The phase lag of DASSC to the M2 velocity (θ_ω) strongly controls the absolute value of F4. F5 accounts for nearly 25% of F1, being mainly attributed to the interaction between the M2 velocity and the M2 elevation. Because of the balance of landward Lagrangian flux (F1+F2) and seaward tidal pumping (mainly in F4), the total flux is towards the land and has a reduced value in the order of 0.1 kg m^{-1} s^{-1}.

4. Discussion

4.1. Influence of advection

The influence of advection of a horizontal concentration gradient on the DASSC evolution and the HRF can be evaluated by investigating the analytical solutions listed in Eqs. (15)–(20), where advection effects are simply represented by the parameter k. At first, as suggested above, the relative importance of the horizontal advection due to the SSC gradient and the local resuspension can be scaled by k/u_1 and B/h_0, while the increasing ratio of k/u_1 to B/h_0 causes stronger advection effects. Secondly, the detailed influences of k on the eight harmonic terms of the tidal DASSC variation (E1–E8) and the five decomposed terms of HRF (F1–F5) are clarified in Table 1 and Eqs. (16)–(20), and are explained in the Appendix A and B. It is noted that E2 and F4 are more strongly controlled by advection because of the first trivial terms of k/u_1, suggesting a potentially important influence of advection on the semi-diurnal variations of DASSC and the tidal pumping in the total HRF.

In the case of the Jiangsu Coast, China, the landward positive DASSC gradient has a pronounced effect. Here advection was excluded by setting $k=0$, and the DASSC time series and the HRF were calculated by Eqs. (15)–(20). In this way, the system was only driven by local resuspension and deposition.

The resulting DASSC is compared with the best fit prediction (Fig. 6). Without the contributions of advection, the asymmetry of the DASSC during the flood and ebb phases disappears. For the E2 term in Eq. (15) and Table 1, which contributes most of the influence of advection, Fig. 6 shows that, when advection is excluded, its variation has only about half of its original amplitude and the phase is inverse.

The tidally averaged DASSC (E1) and each decomposition term of the suspended sediment flux (F1–F5) are listed in Table 2 as

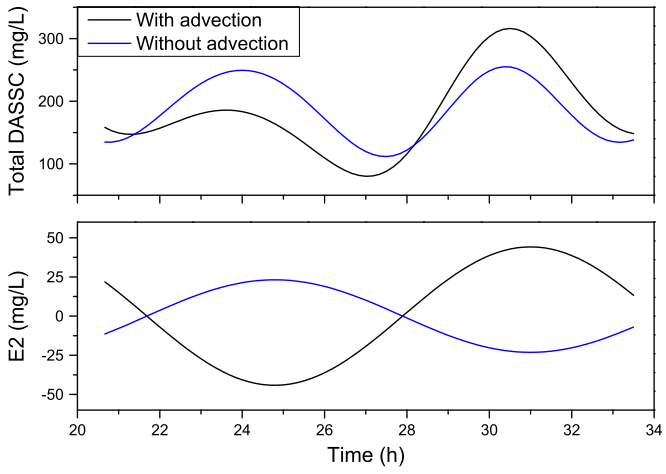

Fig. 6. The different responses of DASSC at the observation site to the conditions with and without the effects of advection induced by the horizontal DASSC gradient. The upper panel shows the total DASSC, the lower panel the E2 decomposition term, which contributes most of the advection influence.

Prediction2. Compared with the best fit results (Prediction1), all of them are similar, except for F4, which reduces from seaward to landward from a value of 0.432 kg m^{-1} s^{-1} to 0.077 kg m^{-1} s^{-1}. This landward tidal pumping (F3+F4+F5) and the landward Lagrangian flux (F1+F2) lead to a large landward total flux (HRF$=-0.578$ kg m^{-1} s^{-1}). These results suggest that, at the observation site, advection induced by the landward positive DASSC gradient plays a crucial role in determining the large seaward F4 and, in turn, the nearly balanced total flux.

Traditionally, tidal pumping is suggested to be mainly due to current asymmetry and sediment lag effects (Uncles and Stephens, 1989; Brenon and Le Hir, 1999). However, the above analysis indicates an important influence of horizontal advection. Thus, when applying the empirical decomposition method to observations (Eq. (1)), care must be taken when interpreting the decomposed terms, especially that of tidal pumping.

4.2. Influence of the deposition coefficient

For a given hydrodynamic condition, the Rouse profile of SSC shows that $C_{bed}/\langle C\rangle H$ is strongly depended on W_s. Based on the definition in Eq. (6), the deposition coefficient D is also mainly controlled by W_s.

There are three important aspects concerning the influence of D. Firstly, it determines the phase lag of DASSC to the forcing factors. The phase lag can be measured by the ratio between the frequency ω_i and the deposition coefficient D (Eqs. (10) and (15)). For coarse-grained sediments having high settling velocities, D is sufficiently larger than ω_i to produce a reduced phase lag. Conversely, for fine-grained sediments having low settling velocities, D is much less than ω_i on account of which a large phase lag is produced. The trend from an in-phase response for coarse sediment to an out-of-phase response for fine sediment indicates the importance of the dimensionless scale ω_i/D, which represents the ratio between the time scale of sediment settling and that of the forcing factor variation. This result is consistent with previous studies (Prandle, 1997; Bass et al., 2002; Stanev et al., 2007; Cheng and Wilson, 2008).

Secondly, the tidally averaged DASSC varies directly with $1/D$ (Eq. (A1)). Thus, low sediment settling velocities produce high mean concentrations, and vice versa. Eq. (15) shows that the amplitudes of the periodic terms (E2–E8) are proportional to $(\omega_i^2+D^2)^{1/2}$. This indicates that varying ranges of DASSC are also inversely related to D.

Thirdly, the phase lag affects the tidal pumping flux. The parameters θ_ω and $\theta_{2\omega}$, which represent the phase lag of SSC to the forcing factors at the M2 and M4 frequencies, respectively, are involved in the formulas of F3–F5. These formulas indicate that the combinations of these phase lags and the phase of the M2 and M4 velocities and the M2 elevation strongly determine the magnitude of tidal pumping.

Two test experiments (Prediction3 and Prediction4) were carried out based on the no-advection prediction (Prediction2) to study the response of changing D (Table 2). Prediction3 and Prediction4 produce a halving and a doubling of D, respectively, but keep two other parameters the same as in Predicton2, in which the advection is excluded. The lag between DASSC and the current velocity decreases with increased D (the upper panel of Fig. 7), and the response of E6 to its forcing factor of the M2 speed shows the same characteristics (the lower panel of Fig. 7). The lower panel also indicates that the amplitude is inversely related to D, but, because of the comparable values of D and ω, the difference in the amplitudes of the three E6 curves is relatively small.

In Table 1, the halving of D results in a doubling of the tidally averaged DASSC (E1) and, consequently, a doubling in the Lagrangian flux (F1+F2). Similarly, the doubling of the D values

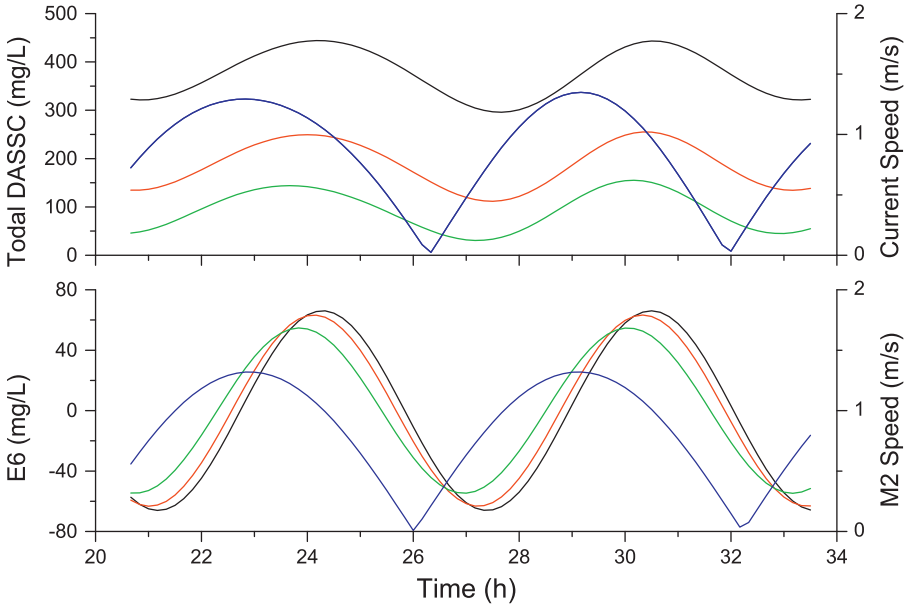

Fig. 7. The response of DASSC at the observation site to different deposition coefficients (D). The upper panel shows the total current speed and the total DASSC, the lower panel the M2 tidal current speed and the E6 decomposition term, which is the largest part of the DASSC variation. The black, red and green curves are associated with Prediction3, Prediction2 and Prediction4 (Table 2), respectively. They have a D of $0.5\times10^{-4}\,s^{-1}$, $1\times10^{-4}\,s^{-1}$, and $2\times10^{-4}\,s^{-1}$, respectively. The blue curves show current speeds. Here the effect of advection is excluded. (For interpretation of the references to color in this figure legend, the reader is referred to the web version of this article.)

lead to a halving of the E1, F1 and F2 values. The absolute values of the pumping terms (F4 and F5) are also inversely related to D, but the response of F4 is more pronounced than that of F5. The experiment with a lower D has a higher landward total suspended sediment flux. This indicates that fine grains have more potential to be transported in the landward direction, thereby contributing to grain-size sorting.

4.3. Applicable scope of the solution

The analytical solution presented in this paper investigates the responses of suspended sediment in a depth-averaged 1D model to the combination of three basic processes: advection of a horizontal DASSC gradient, local resuspension and deposition. After reasonable simplification, the three processes are shown to be controlled by the DASSC gradient k, the resuspension coefficient B, and the deposition coefficient D, respectively. Because of its simplicity, the solution can be easily applied to field observations, thereby providing a more comprehensive understanding of DASSC variation and HRF than the empirical methods of Weeks et al. (1993) and Dyer (1997). The solution can be fitted to the observations at a fixed station in a well-mixed tide-dominated environment, which can be abstracted as a 1D system driven by bidirectional currents, after the three free parameters (k, B and D) have been calibrated.

However, because of its simplicity some processes have been omitted. For example, in connection with sediment deposition, aggregation and disaggregation have been observed in the course of the tidal cycle (Ellis et al., 2004; Jago et al., 2006). This means that the settling velocity is not constant but variable over the tidal cycle. Furthermore, bed consolidation (Dyer, 1995; Anthony et al., 2010), depth-limited erosion (Sanford and Maa, 2001), and bed sediment availability (Velegrakis et al., 1997; Bass et al., 2002) may complicate the local resuspension simulation. Also, stratification effects induced by salinity and/or sediment can significantly influence the water and sediment dynamic behavior (e.g., Geyer, 1993; Wang et al., 2005). Thus, suspended sediment is subject to different advection in different water layers, and this shear diffusion caused by the nonlinear interaction of turbulence and advection may play a substantial role in horizontal suspended sediment transport (e.g., Stanev et al., 2007).

The assumption of a constant DASSC gradient k is a lesser problem. Thus, if a spatial DASSC distribution pattern is available from numerical modeling results (Cheng and Wilson, 2008) and/or multi-site observations, this gradient can be parameterized as a trigonometric Fourier series only associated with time. Then, substituting the series and the parameterized velocities and water depths in Eq. (8), a new solution of Eq. (9) can easily be obtained. Only when such spatial information is not available, as in the case of single site observations, a constant gradient must be assumed in the present solution, which then provides a first order approximation only. It should also be noted that a constant gradient assumption is not suitable for some environments, for example, the central part of the estuarine turbidity maximum, although it would satisfy the areas on either side of it.

It is also noted that only the semi-diurnal and quarter-diurnal components of the tide are involved in the present study, although the suspended sediment concentrations and fluxes (rates and net directions) may also be affected by the other longer periods of the tidal signals, e.g., the spring–neap cycle (Postma, 1967; Schoellhamer, 2002). Because no observations are available over a whole spring–neap cycle, the related responses of concentrations and fluxes are still not entirely clear.

5. Conclusions

Simplified analytical solutions for tidal variations of DASSC and HRF have been obtained for a single site based on a depth-averaged 1D model combined with three basic processes: advection of a horizontal DASSC gradient, local resuspension and deposition. The model is driven by the forcing factors of residual, M2 and M4 current velocities, mean water depth, M2 tidal amplitude and the DASSC gradient. The solution of DASSC consists of eight terms, each of which represent the particular effects of different forcing factors with clear physical meanings, thereby

allowing the empirical decomposition terms of HRF to be formulized and directly interpreted.

The solutions show that potentially there may be important influences of advection on DASSC and HRF, especially the semi-diurnal variations of DASSC and the tidal pumping in the total HRF. The analytical formulas also suggest that the deposition coefficient or the sediment settling velocity plays an important role on determining the phase lag of DASSC to the external forcing factors, the tidally averaged DASSC, and the tidal pumping flux.

The solutions have been successfully applied to fit and explain the observations at a fixed station in a macro-tidal channel located along the Jiangsu Coast, China. The results suggest that the M4 DASSC variation is due to resuspension induced by the M2 velocity, and that the M2 DASSC variation is mainly controlled by advection and, in addition, by resuspension induced by the interaction of the M2 and M4 velocities. The horizontal DASSC gradient leads to a large seaward tidal pumping (F4 term), which is offset by the landward Lagrangian flux that results in a reduced landward HRF.

Acknowledgments

The study was supported by the Senckenberg Institute, the Chinese Scholarship Committee (CSC) and the Natural Science Foundation of China (NSFC, Grant numbers 40876043 and 40830853). Jianjun Jia, Xinqing Zou, Yang Yang, Aijun Wang, and Bingwen Shi participated in the field work. The reviewers' comments are substantially contributed to improving the clarity of the manuscript.

Appendix A. Interpretation of eight harmonic terms in the solution of DASSC

The solution of DASSC in Eq. (15) consists of eight harmonic terms (E1–E8) with the coefficients shown in Table 1, each term corresponding to particular physical processes induced by the forcing factors and their interactions. These factors are residual, M2 and M4 current velocities, mean water depth, M2 tidal amplitude, and the DASSC gradient.

E1 is the SSC averaged over depth and tidal cycle

$$\mathrm{E1} = \overline{\langle C \rangle} = \frac{1}{T}\int_0^T \langle C \rangle dt = \frac{1}{D}\left(-ku_0 + \frac{1}{2}\frac{B}{h_0}u_1^2\right) \tag{A1}$$

The first term $(-ku_0)$ indicates the contribution of horizontal advection by the residual current, causing the averaged DASSC to decrease when the DASSC increases in the direction of the residual velocity, and vice versa. The second term $(Bu_1^2/2h_0)$ is the tidally averaged DASSC induced by local resuspension of the M2 current.

E2, E3 and E4 represent the M2 variations of DASSC but with different phases. E2 has the same phase as the M2 velocity (φ_1). The first term in A_2 $(-ku_1)$ shows an in-phase response of DASSC to the horizontal advection driven by the M2 current, which has been identified by Weeks et al. (1993) as the advective component. The second and third terms are due to the interaction between the residual and the M2 velocity, and that between the M2 velocity and the M2 tidal elevation, respectively. E3 is induced by the interaction of the M2 and M4 currents and thus with the phase of $(\varphi_2-\varphi_1)$. E4 demonstrates the interaction between the M2 velocity and the M2 elevation, having the same phase as the M2 elevation (ϕ).

E5 and E6 have the M4 frequency. E5 shows an in-phase response of DASSC to the horizontal advection driven by the M4 current. E6 is the M4 variation of DASSC induced by the M2 current resuspension and represents the local component in the concept of Weeks et al. (1993). E7 and E8 stand for the M6 variation of the DASSC. E7, as in the case of E3, is also due to the M2 and M4 current interaction, but has a triple frequency and the phase of $(\varphi_2+\varphi_1)$. E8 is another product of the interaction of the M2 velocity and the M2 elevation.

Appendix B. Interpretation of the terms F1–F5 in the solution of HRF

The mechanisms of residual sediment flux can be revealed by the analytical formula of terms F1–F5. Eq. (16) shows that the Eulerian flux F1 is controlled by the residual velocity (u_0) and the tidally averaged DASSC (Eq. (A1)). Eq. (17) shows that the Stokes' drift flux is strongly related to the phase difference between the M2 velocity and the M2 tidal elevation $(\varphi_1-\phi)$ and the amplitude of the M2 tidal elevation. Eq. (18) shows that F3, which is induced by the interaction between the tidal elevations and the DASSC, is a second order trivial term, and has less importance for the total flux. The long formula of F4 in Eq. (19) indicates the complexity of the interaction between velocity and DASSC. The existence of several zero and first order trivial terms in Eq. (19) suggest the probable importance of F4 to the total flux. This characteristic has been supported by field observations. Su and Wang (1986), Li and Chen (1998), Wu et al. (2001) and Ganju et al. (2005) found that this term is not only dominant in the tidal pumping (F3+F4+F5), but is also important for the total flux. The solution indicates the control of the phase lag of DASSC and the phase differences between tidal current and tidal elevation. The first term in Eq. (20), which is the only first order trivial term for F5, shows a strong dependence on the amplitude of the tidal elevation of the M2 tide, the phase differences among the velocity and tidal elevations and the phase lag of DASSC. The involvement of the DASSC gradient (k) in the formulas of F3–F5 suggests an impact of horizontal advection on tidal pumping.

References

Allen, G.P., Salomon, J.C., Bassoullet, P., Du Penhoat, Y., De Grandpre, C., 1980. Effects of tides on mixing and suspended sediment transport in macrotidal estuaries. Sedimentological Geology 26, 69–90.

Amos, C.L., Daborn, G.R., Christian, H.A., Atkinson, A., Robertson, A., 1992. In situ measurements on fine-grained sediments from the Bay of Fundy. Marine Geology 108, 175–196.

Anthony, E.J., Gardel, B., Gratiot, N., Proisy, C., Allison, M.A., Dolique, F., Fromard, F., 2010. The Amazon-influenced muddy coast of South America: a review of mud–bank–shoreline interactions. Earth-Science Reviews 103, 99–121.

Barua, D.K., Kuehl, S.A., Miller, R.L., Moore, W.S., 1994. Suspended sediment distribution and residual transport in the coastal ocean off the Ganges–Brahmaputra river mouth. Marine Geology 120, 41–61.

Bass, S.J., Aldridge, J.N., McCave, I.N., Vincent, C.E., 2002. Phase relationships between fine sediment suspensions and tidal currents in coastal seas. Journal of Geophysical Research 107 (C10), 3146. doi:10.1029/2001JC001269.

Brenon, I., Le Hir, P., 1999. Modelling the turbidity maximum in the Seine Estuary (France): identification of formation processes. Estuarine, Coastal and Shelf Science 49, 525–544.

Cheng, P., Wilson, R.E., 2008. Modeling sediment suspensions in an idealized tidal embayment: importance of tidal asymmetry and settling lag. Estuaries and Coasts 31, 828–842.

Dronkers, J., 1995. Tide-induced residual transport of fine sediment. In: van de Kreeke, J. (Ed.), Physics of Shallow Bays and Estuaries, Miami 1984, Springer Verlag, pp. 228–244.

Dronkers, J., 2005. Dynamics of Coastal Systems. Advanced Series on Ocean Engineering, vol. 25. World Scientific, Singapore, 520 pp.

Dyer, K.R., 1974. The salt balance in stratified estuaries. Estuarine and Coastal Marine Science 2, 273–281.

Dyer, K.R., 1995. Sediment transport processes in estuaries. second ed. In: Perillo, G.M.E. (Ed.), Geomorphology and Sedimentology of Estuaries. Developments in Sedimentology, 53. Elsevier Science, Amsterdam, pp. 423–449.

Dyer, K.R., 1997. Estuaries—Physical Introduction, second ed. John Wiley and Sons, Chichester 195 pp.

Ellis, K.M., Bowers, D.G., Jones, S.E., 2004. A study of the temporal variability in particle size in a high-energy regime. Estuarine, Coastal and Shelf Science 61, 311–315.
Fischer, H.B., 1976. Mixing and dispersion in estuaries. Annual Review of Fluid Mechanics 8, 107–133.
Friedrichs, C.T., Aubrey, D.G., 1988. Non-linear tidal distortion in shallow well mixed estuaries: a synthesis. Estuarine, Coastal and Shelf Science 27, 521–545.
Ganju, N.K., Schoellhamer, D.H., Bergamaschi, B.A., 2005. Suspended sediment fluxes in a tidal wetland: controlling factors, and error analysis. Estuaries 28, 812–822.
Geyer, W.R., 1993. The importance of suppression of turbulence by stratification on the estuarine turbidity maximum. Estuaries 16, 113–125.
Gibbs, R.J., Matthew, M.D., Link, D.A., 1971. The relationship between sphere size and settling velocity. Journal of Sedimentary Petrology 41, 1–18.
Groen, P., 1967. On the residual transport of suspended matter by an alternating tidal current. Netherlands Journal of Sea Research 3–4, 564–574.
Guezennec, L., Lafite, R., Dupont, J.-P., Meyer, R., Boust, D., 1999. Hydrodynamics of suspended particulate matter in the tidal freshwater zone of a macrotidal estuary (the Seine Estuary, France). Estuaries 22, 717–727.
Hill, P.S., McCave, I.N., 2001. Suspended particle transport in benthic boundary layers. In: Boudreau, B.P., Jorgensen, B.B. (Eds.), The Benthic Boundary Layer: Transport Processes and Biogeochemistry. Oxford Univ. Press, New York, pp. 78–103.
Hill, D.C., Jones, S.E., Prandle, D., 2003. Derivation of sediment resuspension rates from acoustic backscatter time-series in tidal waters. Continental Shelf Research 23, 19–40.
Hoitink, A.J.F., Hoekstra, P., van Maren, D.S., 2003. Flow asymmetry associated with astronomical tides: implications for the residual transport of sediment. Journal of Geophysical Research 108 (C10), 3315. doi:10.1029/2002JC001539.
Jago, C.F., Jones, S.E., 1998. Observation and modelling of the dynamics of benthic fluff resuspended from a sandy bed in the southern North Sea. Continental Shelf Research 18, 1255–1282.
Jago, C.F., Jones, S.E., Sykes, P., Rippeth, T., 2006. Temporal variation of suspended particulate matter and turbulence in a high energy, tide-stirred, coastal sea: relative contributions of resuspension and disaggregation. Continental Shelf Research 26, 2019–2028.
Jay, D.A., Geyer, W.R., Uncles, R.J., Vallino, J., Largier, J., Boynton, W.R., 1997. A review of recent developments in estuarine scalar flux estimation. Estuaries 20, 262–280.
Krivtsov, V., Gascoigne, J., Jones, S.E., 2008. Harmonic analysis of suspended particulate matter in the Menai Strait (UK). Ecological Modelling 21, 53–67.
Le Hir, P., Ficht, A., Jacinto, R.S., Lesueur, P., Dupont, J.-P., Lafite, R., Brenon, I., Thouvenin, B., Cugier, P., 2001. Fine sediment transport and accumulations at the mouth of the Seine Estuary (France). Estuaries 24, 950–963.
Li, J., Chen, Z., 1998. Sediment resuspension and implications for turbidity maximum in the Changjiang Estuary. Marine Geology 148, 117–124.
Pino Q, M., G.M.E., Perillo, P., Santamarina, 1994. Residual fluxed in a cross-section of the Valdivia River Estuary, Chile. Estuarine, Coastal and Shelf Science 38, 491–505.
Postma, H., 1961. Transport and accumulation of suspended matter in the Dutch Wadden Sea. Netherlands Journal of Sea Research 1, 148–190.
Postma, H., 1967. Sediment transport processes in estuaries. In: Lauff, G.H. (Ed.), Estuaries, AAAS Publication No. 83, pp. 158–179.
Prandle, D., 1997. Tidal characteristics of suspended sediment concentrations. Journal of Hydraulic Engineering 123, 341–350.
Pritchard, D., 2005. Suspended sediment transport along an idealised tidal embayment: settling lag, residual transport and the interpretation of tidal signals. Ocean Dynamics 55, 124–136.
Sanford, L.P., Halka, J.P., 1993. Assessing the paradigm of mutually exclusive erosion and deposition of mud, with examples from upper Chesapeake Bay. Marine Geology 114, 37–57.
Sanford, L.P., Maa, J.P.-Y., 2001. A unified erosion formulation for fine sediments. Marine Geology 179, 9–23.
Schoellhamer, D.H., 2002. Variability of suspended-sediment concentration at tidal to annual time scales in San Francisco Bay, USA. Continental Shelf Research 22, 1857–1866.
Soulsby, R.L., 1997. Dynamics of Marine Sands. Thomas Telford, Oxford 249 pp.
Stanev, E.V., Brink-Spalink, G., Wolff, J.-O., 2007. Sediment dynamics in tidally dominated environments controlled by transport and turbulence: a case study for the East Frisian Wadden Sea. Journal of Geophysical Research 112, C04018. doi:10.1029/2005JC003045.
Sternberg, R.W., Larsen, L.H., Miao, Y.T., 1985. Tidally driven sediment transport on the East China Sea continental. Continental Shelf Research 4, 105–120.
Su, J.L., Wang, K.S., 1986. The suspended sediment balance in Changjiang estuary. Estuarine, Coastal and Shelf Science 23, 81–98.
Tian, T., Merico, A., Su, J., Staneva, J., Wiltshire, K., Wirtz, K., 2009. Importance of resuspended sediment dynamics for the phytoplankton spring bloom in a coastal marine ecosystem. Journal of Sea Research 62, 214–228.
Uncles, R.J., Elliott, R.C.A., Weston, S.A., 1985a. Dispersion of salt and suspended sediment in a partly mixed estuary. Estuaries 8, 256–269.
Uncles, R.J., Elliott, R.C.A., Weston, S.A., 1985b. Observed fluxes of water, salt and suspended sediment in a partly mixed estuary. Estuarine, Coastal and Shelf Science 20, 147–167.
Uncles, R.J., Stephens, J.A., 1989. Distributions of suspended sediment at high water in a macrotidal estuary. Journal of Geophysical Research 94, 14395–14405.
Uncles, R.J., Stephens, J.A., 1993. Nature of the turbidity maximum in the Tamar Estuary, UK. Estuarine, Coastal and Shelf Science 36, 413–431.
van de Kreeke, J., Day, C.M., Mulder, H.P.J., 1997. Tidal variations in suspended sediment concentration in the Ems estuary: origin and resulting sediment flux. Journal of Sea Research 38, 1–16.
van de Kreeke, J., Hibma, A., 2005. Observations on silt and sand transport in the throat section of the Frisian Inlet. Coastal Engineering 52, 159–175.
van de Kreeke, J., Robaczewska, K., 1993. Tide-induced residual transport of coarse sediment; application to the Ems estuary. Netherlands Journal of Sea Research 31, 209–220.
van Ledden, M., Wang, Z.B., Winterwerp, H., de Vriend, H., 2004. Sand–mud morphodynamics in a short tidal basin. Ocean Dynamics 54, 385–391.
van Maren, D.S., Hoekstra, P., Hoitink, A.J.F., 2004. Tidal flow asymmetry in the diurnal regime: bed-load transport and morphologic changes around the Red River Delta. Ocean Dynamics 54, 424–434.
Velegrakis, A.F., Gao, S., Lafite, R., Dupont, J.P., Huault, M.F., Nash, L.A., Collins, M.B., 1997. Resuspension and advection processes affecting suspended particulate matter concentrations in the central English Channel. Journal of Sea Research 38, 17–34.
Wang, X.H., Byun, D.S., Wang, X.L., Cho, Y.K., 2005. Modelling tidal currents in a sediment stratified idealized estuary. Continental Shelf Research 25, 655–665.
Weeks, A.R., Simpson, J.H., Bowers, D.B., 1993. The relationship between concentrations of suspended particulate material and tidal processes in the Irish Sea. Continental Shelf Research 13, 1325–1334.
Wu, J.-X., Shen, H.-T., Xiao, C.-Y., 2001. Sediment classification and estimation of suspended sediment fluxes in the Changjiang Estuary, China. Water Resources Research 37, 1969–1979.
Xin, F., Wang, Y., Gao, J., Zou, X., 2010. Seasonal distributions of the concentrations of suspended sediment along Jiangsu Coastal Sea. Oceanological et Limnologia Sinica 41, 459–468 (in Chinese with English abstract).
Yang, Z., Hamrick, J.M., 2003. Variational inverse parameter estimation in a cohesive sediment transport model: an adjoint approach. Journal of Geophysical Research 108 (C2), 3055. doi:10.1029/2002JC001423.
You, Z.J., 2005. Estimation of bed roughness from mean velocities measured at two levels near the seabed. Continental Shelf Research 25, 1043–1051.
Yu, Q., Flemming, B.W., Gao, S., 2011. Tide-induced vertical suspended sediment concentration profiles: phase lag and amplitude attenuation. Ocean Dynamics 61, 403–410.